HHS Public Access

Author manuscript

Toxicol Appl Pharmacol. Author manuscript; available in PMC 2015 October 01.

Published in final edited form as:

Toxicol Appl Pharmacol. 2014 October 1; 280(1): 86–96. doi:10.1016/j.taap.2014.07.012.

Hydroxychavicol, a betel leaf component, inhibits prostate cancer through ROS-driven DNA damage and apoptosis

Sushma Reddy Gundala[1], **Chunhua Yang**[1], **Rao Mukkavilli**[2], **Rutugandha Paranjpe**[1,^], **Meera Brahmbhatt**[1,^], **Vaishali Pannu**[1], **Alice Cheng**[1], **Michelle D. Reid**[3], and **Ritu Aneja**[1]

[1]Department of Biology, Georgia State University, Atlanta, GA-30303

[2]Advinus Therapeutics, Karnataka, India

[3]Department of Pathology, Emory University School of Medicine, Atlanta, GA, USA

Abstract

Dietary phytochemicals are excellent ROS-modulating agents and have been shown to effectively enhance ROS levels beyond toxic threshold in cancer cells to ensure their selective killing while leaving normal cells unscathed. Here we demonstrate that hydroxychavicol (HC), extracted and purified from Piper betel leaves, significantly inhibits growth and proliferation via ROS generation in human prostate cancer, PC-3 cells. HC perturbed cell-cycle kinetics and progression, reduced clonogenicity and mediated cytotoxicity by ROS-induced DNA damage leading to activation of several pro-apoptotic molecules. In addition, HC treatment elicited a novel autophagic response as evidenced by the appearance of acidic vesicular organelles and increased expression of autophagic markers, LC3-IIb and beclin-1. Interestingly, quenching of ROS with tiron, an antioxidant, offered significant protection against HC-induced inhibition of cell growth and down regulation of caspase-3, suggesting the crucial role of ROS in mediating cell death. The collapse of mitochondrial transmembrane potential by HC further revealed the link between ROS generation and induction of caspase-mediated apoptosis in PC-3 cells. Our data showed remarkable inhibition of prostate tumor xenografts by ~72% upon daily oral administration of 150 mg/kg bw HC by quantitative tumor volume measurements and non-invasive real-time bioluminescent imaging. HC was well-tolerated at this dosing level without any observable toxicity. This is the first report to demonstrate the anti-prostate efficacy of HC *in vitro* and *in vivo*, which is perhaps attributable to its selective prooxidant activity to eliminate cancer cells thus providing compelling grounds for future preclinical studies to validate its potential usefulness for prostate cancer management.

*Correspondence be addressed to: Ritu Aneja, Department of Biology, Georgia State University, Atlanta, GA-30303 raneja@gsu.edu; Phone: 404-413-5417; Fax: 404-413-5301.

^All authors contributed equally

Conflict of Interest Statement: None declared.

Keywords

Hydroxychavicol; reactive oxygen species (ROS); apoptosis; DNA damage; autophagy; prostate cancer

INTRODUCTION

Polyphenols are major class of phytochemicals known for their disease-fighting and stress-defeating properties. The emerging hypothesis of Xenohormesis, a phenomenon by which polyphenols resist stress, combat disease, and confer health benefits (Howitz and Sinclair, 2008; Hooper *et al.*, 2010) has propelled the evaluation of the role of reactive oxygen species (ROS) in dictating health benefits exerted by phenolic phytochemicals. Extensive literature describes the two-pronged approach launched by these phenolic compounds, one that regulates chemopreventive benefits by enhancing the antioxidant defenses, while the other confers chemotherapeutic efficacy due to induction of cellular stress (ROS levels) leading to cell death (Lamming *et al.*, 2004; Trachootham *et al.*, 2009a; Surh, 2011). Several studies suggest that cancer cells display higher reactive oxygen species (ROS) concentrations compared to normal cells (Szatrowski and Nathan, 1991; Schumacker, 2006; Trachootham *et al.*, 2009b; Trachootham *et al.*, 2009a) and thus an increase in ROS levels can easily tip off the balance in cancer cells due to their higher baseline levels of ROS to result in cell death (Trachootham *et al.*, 2009a).

Inequalities in basal ROS levels in normal and cancer cells can perhaps be ascribed to increased metabolic activity in the latter, which creates a persistent prooxidative condition (Trachootham *et al.*, 2009a). In cancer cells, while moderate or controlled ROS levels lead to survival adaptations that promote their growth and progression, a further increase to higher levels can induce cell death. Excessive levels of ROS disrupt the redox balance maintained in cancer cells by either irreversibly damaging cellular macromolecules including carbohydrates, lipids, proteins and DNA or by interfering with the regulation of redox signaling proteins at transduction or transcriptional levels (Gibellini, 2010a). Cancer cells can succumb to death due to these high ROS levels via several mechanisms including apoptosis, necrosis, autophagy, mitotic catastrophe, and even due to the loss of drug-resistance adaptation (Surh, 2003). Intrinsically driven apoptosis due to excess ROS is mediated directly through the mitochondria and involves the opening of permeability transition (PT) pore complex followed by release of cytochrome c into the cytosol, which triggers the caspase cascade culminating in cell death (Gibellini, 2010b). Thus, drugs that act as prooxidants and tip over the ROS balance in cancer cells by promoting the leakage of free radicals from the mitochondria may prove to be valuable anticancer therapeutics. Although plant phenolics have been long known to have antioxidant functions, their role in enhancing ROS levels is emerging.

Chemically, polyphenols are redox moieties and this property confers on them the unique dual ability to quench as well as generate ROS (Decker, 1997; Sakihama *et al.*, 2002). The chemopreventive efficacy of certain polyphenols lies in their antioxidant properties and their ability to scavenge ROS thereby reducing oxidative stress. Such species at low concentration

and in normal cells would act as chemopreventive agents (Bouayed and Bohn, 2010; Surh, 2011). Other species of polyphenols can act as prooxidants and generate ROS. The ROS surge induces DNA damage and eventually apoptosis thereby exerting a potential chemotherapeutic action (Martin and Barrett, 2002; Trachootham *et al.*, 2009a). Such species are effective at higher concentrations in cells with higher levels of oxidative stress (Azam *et al.*, 2004). Literature suggests that polyphenols with catechol and/or pyrogallol groups can exhibit prooxidant properties, either by reducing iron (III) or copper (II) ions while chelation or by the reaction of ortho-hydroxyphenoxy radical, produced from their oxidation, with other free-radical species to oxidize ortho-quinones and O_2^- (Mira *et al.*, 2002). Thus, the unique properties that include relative abundance in nature, lack of selectivity-related side effects, and patient compliance, which potentially underscore their anticancer benefits, have kindled a lot of interest in the recent times to further investigate the phenolic phytochemicals.

We have recently reported the bioactive constituents of *Piper betel* leaf extract (BLE), and its significant antiproliferative activity in *in vitro* and *in vivo* prostate cancer models (Paranjpe *et al.*, 2013). Our study concluded that the phenolic compound, hydroxychavicol (HC) is the most abundant phytochemical in betel leaves that majorly contributed to the antiproliferative efficacy of BLE. Although HC is present at ~26%, vital factors like environment, cultivation, harvest period, extraction procedures etc, may greatly influence its relative abundance (Quideau *et al.*, 2011; Sasidharan *et al.*, 2011). To identify the optimal concentration at which HC imparts maximum anticancer efficacy and further evaluate its pharmacological significance, it is essential to isolate and purify HC from betel leaves.

Literature reports suggest that HC is effective in impeding cell cycle progression of prostate cancer and oral KB carcinoma cells (Chang *et al.*, 2002; Chang *et al.*, 2007). Also, HC has been shown to impart anti-mutagenicity (Amonkar *et al.*, 1986; Bhide *et al.*, 1991a; Bhide *et al.*, 1991b; Kumar, 2010), antiulcerogenic (Bhattacharya *et al.*, 2005; Sarkar *et al.*, 2008), and antioxidative (Chen *et al.*, 2000; Bhattacharya *et al.*, 2005) properties specifically against cancer cells. There have also been speculations regarding its stress-inducing properties (Chen *et al.*, 2000; Chang *et al.*, 2002). However, there is a dearth of data emphasizing the *in vivo* efficacy of HC and its prooxidant nature in prostate cancer cells, which could potentially lead to its development as a single-agent chemotherapeutic agent or in an adjuvant setting. Here we report the prooxidant property of HC obtained from betel leaves, as well as its anticancer mechanisms in *in vitro* and *in vivo* prostate cancer models emphasizing the HC-induced ROS effects on various pathways.

MATERIALS AND METHODS

Cell culture, chemicals and reagents

Piper betel leaves were purchased from the local farmer's market in Atlanta, GA. Dichloromethane (DCM), and methanol (MeOH) were obtained from Fisher Scientific (Pittsburgh, PA). The silica used for classical chromatography was from EMD Biosciences (Billerica, MA). Thin-layer chromatography (TLC) plates were from EMD chemicals (Billerica, MA). Androgen-independent prostate cancer cells, PC-3, DU145, C4-2 and 22Rv1 were purchased from American Type Culture Collection (ATCC, Manassas, VA)

were cultured in RPMI-1640 media supplemented with 10% heat-inactivated fetal bovine serum (FBS) and 5% penicillin/streptomycin. The normal prostate epithelial, RWPE-1 cells purchased from American Type Culture Collection (ATCC, Manassas, VA) were cultured in Keratinocyte-SFM medium kit (Invitrogen, Grand Island, NY) supplemented with 10% heat-inactivated fetal bovine serum (FBS).

Luciferase-expressing PC-3 cells (PC3-luc) were from PerkinElmer (Hopkinton, MA) and were maintained in MEM medium with 10% FBS, Hyclone, (Pittsburgh, PA). All the cell lines were made sure to be devoid of mycoplasma contamination using Universal Mycoplasma Detection Kit from ATCC (ATCC, Cat#30-1012K, Manassas, VA). The MTT dye (thiazolyl blue tetrazolium bromide, 98% TLC), Acridine orange (AO), 2′,7′-dichlorofluorescein diacetate (DCFDA), chloroquine, 3-methyladenine (3-MA), dimethyl sulfoxide (DMSO), Hoechst stain and β-actin antibody were from Sigma (St. Louis, MO). Dihydroethidium (DHE), 4,5-dihydroxy-1, 3-benzenedisulfonic acid disodium salt monohydrate (tiron), 5,5′,6,6′-tetrachloro-1,1′,3,3′-tetraethylbenzimidazolyl carbocyanine iodide (JC-1), apocynin, rotenone and cyclosporin A were from Fisher Scientific. The concentrations of the above reagents used in the study were: 100 μM HC, 25 μg/ml of AO, 5 μM DHE, 25 μM DCFDA, 2.5 μg/ml of JC-1, 0.5 mM 3-MA; 1 mM tiron, 100 nM rotenone, 10 μM apocynin and 5 μM cyclosporin A. Primary antibodies for beclin-1, light chain 3 (LC3IIb), cleaved caspase-3, cleaved PARP, γ-H2AX, and cytochrome c were from Cell Signaling (Beverly, MA). MitoTracker Red, Alexa 488- or 555-conjugated secondary antibodies were from Life Technologies (Grand Island, NY). Horseradish peroxidase-conjugated secondary antibodies were from Santa Cruz Biotechnology, Inc. Hydroxychavicol (HC) was extracted from betel leaves and was characterized for >99% purity.

Isolation of HC from Betel leaves

Freshly chopped Piper betel leaves were submerged in deionized water and extraction was carried out in a boiling apparatus for 3 h followed by collection of the supernatant by filtration for three consecutive days. The pooled supernatant was then concentrated to $1/12^{th}$ of the original volume under reduced pressure at a temperature of 50°C. This concentrated aqueous extract was further extracted 6 times in a separating funnel with 250 ml of DCM each time, followed by vacuum filtration through celite bed. The resultant clear DCM fraction was then concentrated under reduced pressure. The residue was then subjected to silica gel column chromatography (100–200 mesh) where the elution was initiated with a total of 1400 ml of DCM followed by 800 ml of 1% MeOH in DCM. Fractions of 100 ml each were collected and subjected to TLC in DCM:MeOH (19:1). The fractions 4–22 were found to contain pure HC and thus were pooled and concentrated under vacuum. HC was further characterized by spectral analysis for both quantitation and >99% purity via HPLC using similar method as described earlier (Paranjpe *et al.*, 2013).

Antiproliferative MTT assay

Androgen-independent human prostate cancer cells, PC-3, DU145, C4-2 and 22Rv1, were seeded in 96 well plates at a density of 3500 cells per plate. After 24 h of incubation, the medium was aspirated and replaced by media dosed with HC at concentrations of 1, 10, 25,

50, 75, 100 and 250 μM. A primary stock was prepared by dissolving HC in DMSO at a concentration of 25 mM from which a secondary concentration of 250 μM was prepared in media. Further dilutions were made using the secondary stock. A total volume of 100 μl was added to each well. After 48 h, the drug-containing medium was replaced with 100 μl of medium containing MTT (Tetrazolium bromide solution in PBS (5mg/ml)). The yellow thiazoyl groups of MTT are reduced to purple tetrazolium crystals by viable cells, which were dissolved in 100 μl of DMSO after 4 h incubation in dark. The absorbance was recorded at 570 nm on a Spectra Max Plus (Molecular Devices, Sunnyvale, CA) multi-well plate reader.

Trypan blue and colony survival assay

5000 PC-3 cells plated in a six-well format were treated with 100 μM of HC the next day. Following 24 h of HC treatment, cell-proliferation was determined using Trypan blue assay. For the colony assay, PC-3 cells were seeded at appropriate dilutions (~100 cells/well) and were treated with 100 μM HC for 24 h, washed, and replaced with regular RPMI-medium. The crystal-violet colonies (each consisting of at least 50 cells) were counted post fixation with 4% formaldehyde solution.

Measurement of ROS

PC-3 cells were seeded in 96 well plates and after 24 h of incubation, the medium was aspirated and the cells were pre-treated with either DHE (oxidized by ROS into ethidium bromide and fluoresces red) or DCFDA (oxidized by ROS to DCF) for 30 min and then treated with HC at concentrations of 50, 100 and 150 μM. Following treatment for 0.5, 1, 3, 6 and 12 h, the induction of ROS was measured using fluorimetry. Further, fluorescently labeled cells stained with either DHE or DCFDA were analyzed flow cytometrically. Furthermore, DHE and DCFDA stained cells on coverslips were examined using fluorescence microscopy. The source of ROS was determined by fluorimetry in the presence of inhibitors like rotenone, cyclosporine A and apocynin.

Cell-cycle studies

PC-3 cells treated with 100 μM HC for 6, 9, 12, 18, and 24 h, were lysed, centrifuged, washed with ice-cold PBS, fixed in 70% ethanol and stored at 4°C. Pellets were collected, washed twice with PBS and stained with propidium iodide in the presence of RNaseA for 45 min in the dark. Cell cycle profile was analyzed by flow cytometry.

Immunofluorescence Microscopy

PC-3 cells grown on coverslips were treated with 100 μM HC, and/or followed by live staining with MitoTracker (100 nM; Ex:Em::579:599) and were then fixed with ice-cold methanol for 10 min. This was followed by blocking with 2% bovine serum albumin/PBS at 37°C for 1 h. The coverslips were then incubated with γ-H2AX, cleaved PARP, cleaved caspase-3 and cytochrome c antibodies (1:100 dilution) 37°C for 1 h, which were then washed with 2% bovine serum albumin/PBS for 10 min at room temperature and incubated with 1:500 dilution of Alexa 488- (Ex:Em::499:519) or 555- (Ex:Em::553:568) conjugated

secondary antibodies. The coverslips were then mounted with Prolong Gold antifade reagent containing 4′,6-diamidino-2-phenylindole (Invitrogen).

Immunoblotting

Protein lysates were collected from cells treated with or without 100 μM HC and were resolved by SDS-PAGE, followed by a transfer onto polyvinylidene difluoride membrane that was incubated with a primary antibody of choice overnight at 4°C. Appropriate secondary antibody was used followed by visualization of the immune-reactive bands by chemiluminescence detection kit (Pierce). β-actin was loading control. The cleaved caspase-3 (Figure 3Ai) and beclin-1 (Figure 5Bi) protein expressions were developed from the same blot.

Detection and Quantification of Acidic Vesicular Organelles (AVOs)

PC-3 cells grown on coverslips followed by treatment with 100 μM HC for 24 h along with controls were stained with 25 μg/ml of AO for 30 min, washed twice with PBS, and fixed using ice-cold methanol. The mounted coverslips were examined under a Zeiss (Axioplan-2) fluorescence microscope (63X objective) for the presence of AVOs, which were also further, confirmed and quantified by flow cytometry. The fluorescence emissions, green (510–530 nm) and red (650 nm), from 5000 cells obtained by illuminating with blue (488 nm) excitation light were measured using a FACS Calibur flow cytometer. The red:green fluorescence ratio for each cell was obtained using FlowJo software (Millot *et al.*, 1997; Karna *et al.*, 2010).

Electron Microscopy

Cells from control and 100 μM HC-treated samples were collected and fixed for 2 h in 2% paraformaldehyde, 0.1% glutaraldehyde in 0.1 M sodium cacodylate, then fixed for 1.5 h with 1% osmium tetroxide, followed by washing, and staining *en bloc* in 1% aqueous uranyl acetate (pH 3.3) for 1 h. The samples were then washed and dehydrating with a series of ethanol solutions (through 3 × 100%). These were then embedded in Spurr epoxy resin (Electron Microscopy Sciences) of which ultrathin sections were cut on a RMC-MYX ultramicrotome, and examined on a LEO 906e transmission electron microscope after counterstaining with lead citrate.

In vivo tumor growth and bioluminescent imaging

Six-week old male BALB/c nude mice (Harlan Laboratories, Inc., Indianapolis, IN) were subcutaneously injected with PC-3-luc cells (1×10^6) on the right flank. After 15 days, mice with palpable tumors were randomly separated into two groups of six mice each. Control group was fed vehicle (PBS with 0.05% Tween-80, pH=7.4) and the treatment group was fed 150 mg/kg body weight HC (dissolved in PBS with 0.05% Tween-80 (pH=7.4)), by oral gavage daily for 6 weeks. Tumor growth differences between the vehicle- and HC-fed mice were compared by measuring the luciferase activity in live mice via real-time bioluminescent imaging on the IVIS *in vivo* imaging system (PerkinElmer, Inc., Hopkinton, MA) equipped with Live Imaging software. 30 mg/ml luciferin was injected intraperitoneally in mice anesthetized with isoflurane that were imaged with a CCD camera.

Image acquisition was recorded with an integration of 20 s and four binnings of 100 pixels. The relative photon count of the tumors on the mice from vehicle- or HC-treated groups was quantitated twice a week for six weeks, while tumor volumes were measured using a vernier caliper. Institutional IACUC guidelines were strictly followed while performing the animal experiments.

Histopathologic and immunohistochemical analyses

Organs and tumors collected from HC- or vehicle-fed mice after 6 weeks of treatment were formalin-fixed or frozen immediately post-euthanasia. The tumor and organ sections were cut (5 μm) and stained with hematoxylin and eosin (H&E), cleaved caspase-3 and cleaved PARP as described previously (Aneja *et al.*, 2010; Karna *et al.*, 2011). A pathologist performed blind-mannered microscopic evaluation of all the sections. Complete blood count was performed on blood samples collected from vehicle- and HC-fed C47BL6/J mice (3 per group) after consecutive oral administration of vehicle and HC (150 mg/kg bw) for 3 days.

Determination of half-maximal lethal dose (LD_{50}) and acute in vivo toxicity

C47BL6/J mice were fed with very high doses (5g/kg and 2 g/kg bw) of HC and followed by observation of their health conditions. HC was fed to mice at various doses to determine the dose at which 50% of the mice in the HC-fed group are alive (LD_{50}).

Statistical analysis

All the experiments were repeated at least 3 times. Values from quantitative experiments are expressed as the mean ± standard deviation (SD) and were calculated using Microsoft-Excel software. The Student's t-test and a two-way analysis of variance (ANOVA) were performed to determine the differences between the control and treatment groups. P-values <0.05 were considered as statistically significant.

RESULTS

HC inhibits proliferation and perturbs the cell cycle progression of human prostate cancer cells

The long latency time of prostate cancer offers a "wide window" of opportunity for chemopreventive intervention by dietary agents. Thus, we first asked if HC inhibited the growth of various androgen-independent prostate cancer cells in a concentration gradient dependent manner. Our data showed that HC significantly inhibited cellular proliferation of all prostate cancer cells with IC_{50} values in the range of 30–320 μM (Figure 1Ai–Aii). The order of sensitivity was 22Rv1>C4-2>PC-3>DU145, with C4-2 being the most sensitive and DU145 the least. DU145 cells were found to be least sensitive against HC treatment likely due to the expression of MDR (multidrug resistance) phenotype and p-glycoprotein (Pgp) in hormone-independent cancer cells like PC-3 and DU145, which are widely known for inducing drug resistance. The IC_{50} of HC in normal prostate epithelial RWPE cells was found to be 398 μM (Figure 1B), which was ~4–13 fold higher than for cancer cells suggesting that HC specifically targets cancer cells while sparing normal cells. HC exhibited similar antiproliferative activity in other cancer cells like MiaPaCa-2, Panc-1, MDA-MB 231 and HeLa (Figure 1C) with IC_{50} values of 76, 224, 126 and 71 μM respectively.

The resistant cell line against HC (as observed in Figure 1Ai, i.e., highest IC_{50}), PC-3 was selected to further understand HC's mechanisms of action. A trypan blue assay performed to quantitate cell viability upon HC treatment, showed reduced cell viability of PC-3 cells in a time-dependent manner (Figure 1Di). We next performed a clonogenic or colony formation assay that determines the capacity of a cell to proliferate indefinitely upon drug removal to form a colony (Figure 1Dii). While control cells proliferated profusely to produce several colonies, only a fraction of treated cells restored their ability to form colonies (Figure 1Dii) upon treatment with 100 μM HC on the relative clonogenicity. Representative micrographs of colonies in control and HC-treated cells (Figure 1Dii, top right) when counted, quantitated to a ~4-fold reduction in number and size of surviving colonies upon HC treatment.

We next asked if HC-mediated growth suppression was due to its cell-cycle intervention. To this end, we evaluated the effect of HC exposure on cell-cycle kinetics of PC-3 cells over time. Figure 1Ei shows time-course of HC-treatment in a three-dimensional format. HC caused cells to accumulate in the G1 phase as early as 6 h until 24 h, followed by an increase in Sub-G1 population, indicating the possible onset of apoptosis.

HC-induced cell death is ROS dependent

HC has been previously reported to generate reactive oxygen species (ROS) and exhibit prooxidant property in epithelial cancer cells (Lee-Chen *et al.*, 1996; Chang *et al.*, 2002), and hence to test if HC could induce ROS in prostate cancer cells, we stained PC-3 cells with DCFDA and DHE and analyzed them flow cytometrically as well as observed microscopically (Figure 2A–C). DCFDA is cell permeable and it is cleaved intracellularly by non-specific cellular esterases. DCFDA reacts with peroxides to yield the fluorescent product, DCF, which is a direct measure of the peroxides generated. The DCF fluorescence was measured at 485 nm (excitation) and 535 nm (emission). HC-treated cells exhibited a significant increase in DCF staining compared to controls (Figure 2Ai) as well as an increase in mean fluorescence (right shift) at 6 and 9 h compared to the controls (Figure 2Aii). However at 12, 18 and 24 h, the intensity was similar to that of controls suggesting that the induction of peroxides by HC was within 12 h of treatment. The dose-dependent increased induction of ROS levels in PC-3 cells by HC was further confirmed fluorimetrically (Suppl. Fig. 1).

Another ROS probe, DHE, which reacts with superoxides was used to further confirm the generation of ROS due to HC. DHE converts to ethidium bromide upon oxidation and appears in the nucleus as red fluorescence. Microscopical examination of HC-treated PC-3 cells revealed the generation of superoxides by HC (Figure 2Bi). Flow cytometric data also suggested the increase in red fluorescence (right shift, Figure 2Bii), read at 580 nm emission wavelength. There was a slight increase in the mean fluorescence intensity from 6 to 18 h and a significant increase at 24 h post-treatment.

It is well known that mitochondria and NADPH oxidase (NOX) are the major endogenous sources of ROS generation in cancer cells (Sauer *et al.*, 2001; Lee *et al.*, 2006). To this end, we raised a question to delineate the source of ROS generation upon HC treatment. Employing specific inhibitors of these sources, we examined the change in mean

fluorescence intensity of DCFDA upon treating with apocynin (NOX inhibitor) and rotenone (mitochondrial complex I inhibitor) (Karna *et al.*, 2010). Interestingly, we observed that simultaneous treatment of PC-3 cells with both inhibitors (Apo+Rot) significantly ablated endogenous ROS levels. However, despite this quenching upon HC treatment, there was a slight increase in ROS levels (Figure 2C) suggesting a mitochondrial and NOX independent induction of oxidative stress. This could most likely be attributed to the presence of catechol group in HC, known for imparting prooxidant property (Mira *et al.*, 2002; Paranjpe *et al.*, 2013). We then asked if the cell death observed upon treatment with HC was dependent on its ROS-generation activity. To this effect, the cell survival of HC-treated PC-3 cells was measured in the presence and absence of tiron, a ROS scavenger (Karna *et al.*, 2010). There was a significant increase in cell survival (50%) in cells pre-treated with tiron, followed by HC as compared to only HC-treated cells (Figure 2D), thus indicating the involvement of HC-induced ROS in triggering cellular death.

HC-induced ROS trigger mitochondrially-mediated intrinsic apoptosis

Having identified that HC-induced cell death is ROS-dependent, we next evaluated if the it is via apoptosis. Our data showed that treatment of PC-3 cells with HC resulted in increased expression of cleaved caspase-3, further supported by increase in cleaved PARP expression at 18 h of HC treatment (Figure 3A–B) suggesting that HC induces apoptosis. Immunofluorescence micrographs of cells treated with HC also show the enhanced expression of apoptotic markers, cleaved caspase-3 and cleaved PARP (Figure 3Aii and 3Bii) compared to their controls. Furthermore, the pro-apoptotic role of ROS was confirmed by evaluating the cleaved PARP expression in tiron pre-treated (2 h) PC-3 cells that were then subjected to HC treatment. Immunoblot analysis of these lysates demonstrated an increased cleaved PARP expression in case of 12, 18 and 24 h samples as compared to their complementary tiron-treated samples, thus indicating that the HC-induced ROS were involved in triggering apoptosis in PC-3 cells.

It is a well-known fact that the release of cytochrome c into the cytosol due to disruption of mitochondrial membrane triggers intrinsic apoptosis (Tait and Green, 2010). Considering our observation that HC induces mitochondrial ROS, evaluating any possible disturbances in the mitochondrial membrane potential seemed to provide a plausible reason for HC-induced apoptosis in cancer cells. To this effect, we further confirmed intrinsic apoptosis by measuring the collapse of mitochondrial transmembrane potential (Ψm) (Figure 3C) and examining release of mitochondrial cytochrome c into the cytosol (Figure 3D). JC-1, a cationic-dye, characterized by membrane potential-dependent mitochondrial accumulation (Cossarizza *et al.*, 1993), was used to stain cells treated with HC for 6, 9, 12, 18 and 24 h along with control cells and an increase in JC-1 monomeric form indicative of Ψm collapse was observed (Figure 3C). This effect was quantitatively determined using flow-cytometry. As seen in Figure 3C, 100 μM HC-treated cells at 6 h showed a right-shift in the mean-fluorescence intensity of green JC-1 monomers compared to controls and similar trend was observed for other timepoints as well. Furthermore, as disruption of Ψm is known to be followed by alterations in expression of Bcl2 members, we found that at 18 h of HC-treatment, increased the levels of phosphorylated Bcl2 was observed, thus indicating its inactivation, while total Bcl2 levels remained unchanged (Figure 3Di). In addition,

cytochrome c is released into the cytosol from the mitochondria 12 h post-HC treatment, which is illustrated in Figure 3Dii indicating induction of intrinsic apoptosis. The MitoTracker (red) stains the mitochondria and the anti-cytochrome c (green) in the control cells co-localizes with the MitoTracker. However, in the HC-treated cells, the overlay of the triple stained cells (MitoTracker (red), cytochrome c (green) and Hoechst dye (blue)) clearly shows no co-localization and cytochrome c is released from the mitochondria (Figure 3Dii).

HC triggers ROS-dependent DNA damage

Oxidative damage caused by excess ROS has been linked to DNA based modifications like single- and double-strand breaks (Cooke *et al.*, 2003). Based on our observations that the growth arrest in HC-treated cells was ROS dependent, we next asked if HC-induced ROS cause DNA damage in PC-3 cells. To this end, we microscopically examined the HC-treated cells over time for γ-H2AX foci that form around the DNA breakage sites. γ-H2AX is the phosphorylated form of histone H2AX and is a sensitive marker of double-strand breaks, an early indication of chromatin modification (Bonner *et al.*, 2008).

γ-H2AX foci were found in HC-treated cells after treatment for 6, 9, 12, 18, 24 h (data not shown) and their expression seemed to be at maximum at 18 h (Figure 4Ai, Aii). Clearly, control cells lacked γ-H2AX foci indicating that the breaks were induced due to HC exposure. Corroborating this observation, immunoblot analysis of HC- treated cell lysates also confirmed expression of γ-H2AX, as early as 6 h, which further peaked at 18 h (Figure 4B) suggesting an early and time-dependent effect on DNA damage by HC. Having identified HC-induced DNA damage, we next wanted to confirm if this is ROS-dependent. Hence, PC-3 cells were pre-treated for 2 h with tiron, a ROS scavenger, followed by HC-treatment at 9, 18 and 24 h. Approximately 58% decrease in number of cells with γ-H2AX foci was observed at 18 h treatment followed by the attenuation of ROS by tiron (Figure 4Ai, Aii) ($P<0.05$).

HC induces robust autophagy in PC-3 cells

Given that HC induced ROS related mitochondrial damage, we were inquisitive to learn whether HC also induced autophagy in human prostate cancer PC-3 cells. Electron microscopy, the gold standard to identify autophagosomes in the cells (Kondo and Kondo, 2006), was employed to demonstrate the effects of HC on PC-3 cells. Transmission electron microscopy was used to observe the ultrastructures present in control and 100 μM HC-treated cells. Large double-membranous cytoplasmic vacuoles resembling autophagosomes with intracellular organelles entrapped within them were observed in HC-treated cells (Figure 5A, indicated by black arrows). The induction of autophagy by HC was further demonstrated by the immunoblot analysis of HC-treated cell lysates for classic autophagy markers, beclin-1 and LC3-IIb. Increased expression of beclin-1 was observed at 12 h treatment and the expression of converted form of LC3-II was observed to increase over time starting as early as 6 h. This was further supported by the microscopic observations of cells stained for acidic vesicular organelles (AVOs), another characteristic feature of autophagy (Paglin *et al.*, 2001; Karna *et al.*, 2010). Cells treated with HC were visualized using fluorescent microscopy upon staining with acridine orange (AO), a lysomotropic agent. AO, a weak base can cross the biological membrane in an uncharged state and

exhibits green fluorescence. Its protonated form is found in the acidic compartments of cells and has a red fluorescence. As seen in Figure 5C, the control cells showed green fluorescence indicating the lack of acidic vacuoles and on the other hand, HC-treated cells showed red fluorescence signifying the presence of AVOs thus suggesting induction of autophagy. We also evaluated the AO fluorescence flow cytometrically and it was observed that there was a significant right shift in cells treated with HC compared to the control as early as 6 h (Figure 5D). However, at 12 h, the HC-treated cells resembled control cells, as there was no shift in the fluorescence intensity.

Furthermore, to determine if the autophagy induced by HC was ROS-dependent, we performed immunoblot analysis of tiron-pretreated cell lysates. The reduced expression of LC3-IIb in 12, 18 and 24 h HC-treated samples suggested that ROS were required to induce autophagy (Figure 5Bii). However, there was minimal expression of LC3-IIb in the control, which was further observed to decrease in tiron-treated control (Figure 5Bii).

Oral HC feeding significantly inhibits PC-3 tumor-growth

Having identified significant *in vitro* anti-proliferative and pro-apoptotic activity of HC, we were curious to examine the *in vivo* efficacy of HC to inhibit subcutaneous human prostate tumor xenografts implanted in athymic nude mice. A PC-3 cell-line stably-expressing luciferase (PC3-luc), which allowed real-time visualization and non-invasive observation of prostate cancer growth was employed in this study. 150 mg/kg bw HC and vehicle (PBS with 0.05% Tween-80, pH=7.4) were fed daily by oral-gavage for six weeks to the mice in treatment and control groups respectively. Therapeutic responses were evaluated upon quantifying the relative photon counts as revealed by non-invasive bioluminescent imaging (Figure 6Ai), and measuring volumes (Figure 6B) of the tumors in mice from both treatment and controls groups using vernier caliper. Approximately 72% reduction in tumor-volume ($p<0.05$ (n=6, Figure. 6Aii)) observed at week six in HC-treated mice signified time-dependent tumor growth inhibition (Figure 6Ai, ii) compared to vehicle-treated group. Further, tumor-volume measurements showed that oral feeding of HC for six weeks (42 days) decreased tumor-volume by ~75% compared to the control group. Due to tumor over burden, complying with our institutional IACUC guidelines, the mice in control group had to be euthanized by the end of six weeks. Furthermore, tumors were excised upon euthanasia from control and treatment groups at the end point. The therapeutic response observed was further supported by ~3.3-fold difference in the tumor weights (Figure 6C) from control and treatment groups.

In vivo apoptotic response of HC feeding in PC-3-luc tumor xenografts was evaluated for cleaved caspase-3 and cleaved PARP expression using western blot analysis of tumor-lysates. As expected, cleaved caspase-3 and cleaved PARP expression (Figure 6E) was higher in tumors from HC-fed group compared to the control group.

Non-toxic effects of HC

Toxicity, a major burden for prostate cancer patients during chemotherapy or radiotherapy, was barely observed in HC-fed mice, which was confirmed by histopathological analysis of various organs posthumously obtained from treatment and control group mice. There were

no discernible differences in the appearance of intestinal, liver, spleen, lung, kidney, brain, heart, testes, adrenal gland and pancreatic tissues from both groups (Suppl. Fig. 2). Comparative evaluation of serum biochemical indicators like blood urea's nitrogen (BUN), lactate dehydrogenase (LDH), creatinine kinase, and hepatic functional markers (ALT, AST, ALP) revealed similar profiles for both vehicle- and HC-fed groups (Suppl. Fig. 3A). Furthermore, complete blood analysis was performed to compare the blood collected from both HC- and vehicle-fed mice. Evaluation of total count/percentage of various blood components including white blood cells (WBC), red blood cells (RBC), hemoglobin (HGB), neutrophils, lymphocytes, monocytes, basophils, eosinophils and platelets was found to be comparable with no signs of toxicity (Suppl. Fig. 3B).

Half-maximal lethal dose (LD_{50}) and acute in vivo toxicity of HC

In the groups fed with very high doses (5g/kg and 2 g/kg bw) of HC, 100% of the C47BL6/J mice died concluding that HC is toxic at such high doses. Furthermore, upon testing several doses, 560 mg/kg bw of HC resulted in the death of 50% mice confirming the half-maximal lethal dose (LD_{50}).

DISCUSSION

Our enthusiasm to decipher the mechanisms via which several plant phytochemicals exert health-promoting benefits led to the revelation of remarkably congruent yet opposite roles played by these chemicals under different physiological conditions. Recent interest in cancer chemopreventive research using whole foods and their active constituents, alone or in combination with current chemotherapeutic drugs has unfolded the mysterious ways through which nature delivers health benefits to mankind. Plant chemicals have been known to fight oxidative stress by quenching the free radicals responsible for mutations leading to genetic alterations and malignant transformation of initiated cells (Quideau *et al.*, 2011). However, certain phytochemicals also exert prooxidant behavior and when at higher concentrations, they tend to induce generation of reactive oxygen species in the cells (Sakihama *et al.*, 2002; Azam *et al.*, 2004; Quideau *et al.*, 2011). Literature suggests that phenolic compounds containing catechol and pyrogallol moieties (Mira *et al.*, 2002) induce ROS levels in cells and thus dispose chemotherapeutic efficacy by leading to death. Given their abundance in nature, it is ideal to isolate phenolic compounds that can exhibit pleotropic mechanisms from plant extracts and exploit their double-edged behavior. Although there is an ongoing debate on employing whole foods vs single active constituents for chemotherapy/chemoprevention, establishing the mechanisms via which the whole food extracts or their constituent phytochemicals can induce death in cancer cells is of utmost importance.

We have recently reported that HC is the most abundant phenolic compound in betel leaves and also the major contributor of anticancer efficacy of betel leaves (Paranjpe *et al.*, 2013). Thus, the next evident step was to isolate HC from betel leaves and investigate the mechanism via which HC induced cell death in cancer cells. Our data demonstrates the *in vitro* anticancer efficacy of HC specifically in various human prostate cancer cell lines like C4-2, DU145, 22Rv1 and PC-3 (Figure 1Ai–Aii) compared to normal prostate epithelial cells, RWPE-1 (Figure 1B). Furthermore, HC also exhibits antiproliferative activity against

a variety of cancer cell lines including MiaPaCa-2 (pancreatic), Panc-1 (pancreatic), MDA-MB-231 (breast) and HeLa (cervical). The cell cycle arrest induced by HC in PC-3 cells (Figure 1Ei–Eii) further supported HC's therapeutic efficiency.

Literature reports suggest that cancer cells possess higher concentrations of reactive oxygen species (ROS) compared to normal cells (Szatrowski and Nathan, 1991; Schumacker, 2006; Trachootham *et al.*, 2009b). While moderate levels of ROS are understood to facilitate cell proliferation and survival, an increase in these levels in cancer cells beyond a threshold lead to cell death. As such, with a low basal level of ROS, normal cells maintain a redox balance between generation and elimination of free radicals, and thus can tolerate a minimal increase in this level. In contrast, cancer cells with high basal levels of ROS have reduced margin to sustain the elevation in these levels. In such a case, an exogenous interference by ROS-modulating agents might enhance the levels beyond toxic threshold, leading to their cell death. This 'weakness' of the cancer cells ensures their selective killing via ROS-mediated mechanisms sparing the normal cells. Thus, drugs acting as prooxidants promoting the leakage of free radicals from the mitochondria prove to be valuable anticancer therapeutics. Although plant phenolics have been long known be antioxidants, their role in enhancing ROS levels is emerging (Donadelli *et al.*, 2011). To the best of our knowledge, no studies have yet shown the prooxidant behavior of HC in human prostate cancer, PC-3 cells experimentally. Our data showed that HC induced peroxides and superoxides in a time-dependent manner (Figure 2). Immunofluorescence staining suggested that green fluorescence in case of DCFDA indicated the induction of peroxides (Figure 2Ai) and red fluorescence in case of DHE signified the induction of superoxides (Figure 2Bi). Flow cytometry using the above-mentioned dyes, further confirmed the time-dependent induction of ROS by HC (Figure 2Aii and Bii). Further investigation revealed that these HC-induced ROS triggered cellular death in PC-3 cells (Figure 2D).

Excessive ROS in cells are known to induce DNA damage, apoptosis and even autophagy, eventually leading to death (Karna *et al.*, 2010). Insights into molecular mechanisms reveal the death-inducing effects of HC-induced ROS in PC-3 cells where treatment with HC led to increase in the expression of cleaved caspase-3 and cleaved PARP in the presence and absence of ROS inhibitor, tiron (Figure 3A). Apoptosis thus induced was intrinsic in nature, suggesting a largely mitochondrially-mediated phenomenon, associated with collapse of transmembrane potential resulting in the expulsion of apoptogenic molecules, as an upregulation in the expression of Bcl-2 and release of cytochrome c levels into the cytosol was observed upon treating with HC (Figure 3C–D). It was also observed that the HC-induced ROS caused DNA damage, as signified by the increase in the expression of γ-H2AX foci that form around the DNA breakage sites (Figure 4). Additionally, these ROS also induced autophagy in HC-treated PC-3 cells (Figure 5).

Autophagy is a type II programmed cell death, which in some cases precedes apoptosis (Chen *et al.*, 2010). At a basal level, autophagy functions in maintaining the cellular homeostatis, but when stimulated by the cellular stress conditions like oxidative stress, it becomes upregulated rapidly. Our observations including the appearance of organelles engulfed in double-membrane bound vesicles (Figure 5A), AVOs (Figure 5C) and overexpression of beclin-1 and LC-3IIb (Figure 5B) revealed that HC-induced ROS

triggered the induction of autophagy in PC-3 cells. Sometimes, under such 'stressed' conditions, autophagy functions as a double-edged sword, contributing to cell survival by engulfing the damaged organelles. When it is unregulated, it leads to cell death by excessive digestion and degradation of cellular components (Kroemer and Levine, 2008; Dewaele *et al.*, 2010). On the other hand, apoptosis, the type I programmed cell death involving the activation of catalytic proteases, leads to rapid destruction of cellular structures. Studies have reported a crosstalk between these 'self-eating' and 'self-killing' mechanisms, due to mutual control of the autophagic and apoptotic proteins in the cell (Maiuri *et al.*, 2007). In this context, we are currently investigating the HC-induced ROS-dependent interplay between autophagy and apoptosis to impact cellular outcomes in prostate cancer cells.

Furthermore, our *in vivo* investigation revealed the remarkable tumor growth inhibition efficacy of HC, also accompanied by non-toxicity (Figure 6, Suppl. Fig. 2 and 3). To assess the safety of HC, the hematologic and histopathological toxicities were evaluated and there were no deviations in the hematologic attributes in samples from treated mice compared to the controls. Using the body surface area normalization method (Reagan-Shaw *et al.*, 2008), we hypothesized the use of HC as a potential chemotherapeutic or chemopreventive agent in humans, where the human equivalent dose of 150 mg/kg *in vivo* dose equals ~12 mg/kg. For an average, 70 kg adult, this is translated to an equivalent dose of <1 g HC, which can be easily supplemented as a part of daily diet.

In conclusion, our study is the first to underline the remarkable prooxidant role of Hydroxychavicol, an active constituent abundant in betel leaves to confer maximum therapeutic benefits as it induces ROS in human prostate cancer cells thus leading to their death. Our observations of this possible prooxidant role of HC are indispensible and provide stimulus to further investigate its chemotherapeutic potential and a possible role in chemoprevention and prostate cancer management.

Supplementary Material

Refer to Web version on PubMed Central for supplementary material.

Acknowledgments

This study was supported by grants to RA from the National Cancer Institute at the National Institutes of Health (R00CA131489, R01 CA169127) and American Cancer Society (121728-RSG-12-004-01-CNE).

ABBREVIATIONS

ROS	reactive oxygen species
HC	hydroxychavicol
BLE	betel leaf extract
FBS	fetal bovine serum
ATCC	American type cell culture
MTT	tetrazolium bromide solution

DNA	deoxyribonucleic acid
LC3-IIb	light chain 3-IIb
DMSO	dimethylsulfoxide
IC_{50}	inhibitory concentration 50%
LC-MS/MS	liquid chromatography tandem mass spectrometry
PT	permeability transition pore complex
AO	acridine orange
LD_{50}	lethal dose 50%
AVOs	acidic vesicular organelles

References

Amonkar AJ, Nagabhushan M, D'Souza AV, Bhide SV. Hydroxychavicol: a new phenolic antimutagen from betel leaf. Food and chemical toxicology: an international journal published for the British Industrial Biological Research Association. 1986; 24:1321–1324. [PubMed: 3100406]

Aneja R, Miyagi T, Karna P, Ezell T, Shukla D, Vij Gupta M, Yates C, Chinni SR, Zhau H, Chung LW, Joshi HC. A novel microtubule-modulating agent induces mitochondrially driven caspase-dependent apoptosis via mitotic checkpoint activation in human prostate cancer cells. European journal of cancer. 2010; 46:1668–1678. [PubMed: 20303260]

Azam S, Hadi N, Khan NU, Hadi SM. Prooxidant property of green tea polyphenols epicatechin and epigallocatechin-3-gallate: implications for anticancer properties. Toxicology in vitro: an international journal published in association with BIBRA. 2004; 18:555–561. [PubMed: 15251172]

Bhattacharya S, Subramanian M, Roychowdhury S, Bauri AK, Kamat JP, Chattopadhyay S, Bandyopadhyay SK. Radioprotective property of the ethanolic extract of Piper betel Leaf. Journal of radiation research. 2005; 46:165–171. [PubMed: 15988134]

Bhide, SV.; Padma, PR.; Amonkar, AJ. IARC scientific publications. 1991a. Antimutagenic and anticarcinogenic effects of betel leaf extract against the tobacco-specific nitrosamine 4-(N-nitrosomethylamino)-1-(3-pyridyl)-1-butanone (NNK); p. 520-524.

Bhide SV, Zariwala MB, Amonkar AJ, Azuine MA. Chemopreventive efficacy of a betel leaf extract against benzo[a]pyrene-induced forestomach tumors in mice. Journal of ethnopharmacology. 1991b; 34:207–213. [PubMed: 1795525]

Bonner WM, Redon CE, Dickey JS, Nakamura AJ, Sedelnikova OA, Solier S, Pommier Y. GammaH2AX and cancer. Nature reviews Cancer. 2008; 8:957–967.

Bouayed J, Bohn T. Exogenous antioxidants - Double-edged swords in cellular redox state: Health beneficial effects at physiologic doses versus deleterious effects at high doses. Oxidative medicine and cellular longevity. 2010; 3:228–237. [PubMed: 20972369]

Chang MC, Uang BJ, Tsai CY, Wu HL, Lin BR, Lee CS, Chen YJ, Chang CH, Tsai YL, Kao CJ, Jeng JH. Hydroxychavicol, a novel betel leaf component, inhibits platelet aggregation by suppression of cyclooxygenase, thromboxane production and calcium mobilization. British journal of pharmacology. 2007; 152:73–82. [PubMed: 17641677]

Chang MC, Uang BJ, Wu HL, Lee JJ, Hahn LJ, Jeng JH. Inducing the cell cycle arrest and apoptosis of oral KB carcinoma cells by hydroxychavicol: roles of glutathione and reactive oxygen species. British journal of pharmacology. 2002; 135:619–630. [PubMed: 11834609]

Chen CL, Chi CW, Liu TY. Enhanced hydroxychavicol-induced cytotoxic effects in glutathione-depleted HepG2 cells. Cancer letters. 2000; 155:29–35. [PubMed: 10814876]

Chen Y, Azad MB, Gibson SB. Methods for detecting autophagy and determining autophagy-induced cell death. Can J Physiol Pharmacol. 2010; 88:285–295. [PubMed: 20393593]

Cooke MS, Evans MD, Dizdaroglu M, Lunec J. Oxidative DNA damage: mechanisms, mutation, and disease. FASEB journal: official publication of the Federation of American Societies for Experimental Biology. 2003; 17:1195–1214. [PubMed: 12832285]

Cossarizza A, Baccarani-Contri M, Kalashnikova G, Franceschi C. A new method for the cytofluorimetric analysis of mitochondrial membrane potential using the J-aggregate forming lipophilic cation 5,5′,6,6′-tetrachloro-1,1′,3,3′-tetraethylbenzimidazolcarbocyanine iodide (JC-1). Biochemical and biophysical research communications. 1993; 197:40–45. [PubMed: 8250945]

Decker EA. Phenolics: prooxidants or antioxidants? Nutrition reviews. 1997; 55:396–398. [PubMed: 9420450]

Dewaele M, Maes H, Agostinis P. ROS-mediated mechanisms of autophagy stimulation and their relevance in cancer therapy. Autophagy. 2010; 6:838–854. [PubMed: 20505317]

Donadelli M, Dando I, Zaniboni T, Costanzo C, Dalla Pozza E, Scupoli MT, Scarpa A, Zappavigna S, Marra M, Abbruzzese A, Bifulco M, Caraglia M, Palmieri M. Gemcitabine/cannabinoid combination triggers autophagy in pancreatic cancer cells through a ROS-mediated mechanism. Cell Death Dis. 2011; 2:e152. [PubMed: 21525939]

Gibellini L, Pinti M, Nasi M, Biasi SD, Roat E, Bertoncelli L, Cossarizza A. Interfering with ROS metabolism in cancer cells: the potential role of Quercetin. Cancers. 2010a:1288–1311. [PubMed: 24281116]

Gibellini L, Pinti M, Nasi M, Biasi SD, Roat E, Bertoncelli L, Cossarizza A. Interfering with ROS metabolism in cancer cells: the potential role of Quercetin. Cancers. 2010b; 2:1288–1311. [PubMed: 24281116]

Hooper PL, Hooper PL, Tytell M, Vigh L. Xenohormesis: health benefits from an eon of plant stress response evolution. Cell stress & chaperones. 2010; 15:761–770. [PubMed: 20524162]

Howitz KT, Sinclair DA. Xenohormesis: sensing the chemical cues of other species. Cell. 2008; 133:387–391. [PubMed: 18455976]

Karna P, Gundala SR, Gupta MV, Shamsi SA, Pace RD, Yates C, Narayan S, Aneja R. Polyphenol-rich sweet potato greens extract inhibits proliferation and induces apoptosis in prostate cancer cells in vitro and in vivo. Carcinogenesis. 2011; 32:1872–1880. [PubMed: 21948980]

Karna P, Zughaier S, Pannu V, Simmons R, Narayan S, Aneja R. Induction of reactive oxygen species-mediated autophagy by a novel microtubule-modulating agent. The Journal of biological chemistry. 2010; 285:18737–18748. [PubMed: 20404319]

Kondo Y, Kondo S. Autophagy and cancer therapy. Autophagy. 2006; 2:85–90. [PubMed: 16874083]

Kroemer G, Levine B. Autophagic cell death: the story of a misnomer. Nat Rev Mol Cell Biol. 2008; 9:1004–1010. [PubMed: 18971948]

Kumar N, Misra P, Dube A, Bhattacharya S, Dikshit M, Ranade S. Piper betle Linn. a maligned Pan-Asiatic plant with an array of pharmacological activities and prospects for drug discovery. Current Science. 2010; 99:922–932.

Lamming DW, Wood JG, Sinclair DA. Small molecules that regulate lifespan: evidence for xenohormesis. Molecular microbiology. 2004; 53:1003–1009. [PubMed: 15306006]

Lee SB, Bae IH, Bae YS, Um HD. Link between mitochondria and NADPH oxidase 1 isozyme for the sustained production of reactive oxygen species and cell death. The Journal of biological chemistry. 2006; 281:36228–36235. [PubMed: 17015444]

Lee-Chen SF, Chen CL, Ho LY, Hsu PC, Chang JT, Sun CM, Chi CW, Liu TY. Role of oxidative DNA damage in hydroxychavicol-induced genotoxicity. Mutagenesis. 1996; 11:519–523. [PubMed: 8921515]

Maiuri MC, Zalckvar E, Kimchi A, Kroemer G. Self-eating and self-killing: crosstalk between autophagy and apoptosis. Nat Rev Mol Cell Biol. 2007; 8:741–752. [PubMed: 17717517]

Martin KR, Barrett JC. Reactive oxygen species as double-edged swords in cellular processes: low-dose cell signaling versus high-dose toxicity. Human & experimental toxicology. 2002; 21:71–75. [PubMed: 12102499]

Millot C, Millot JM, Morjani H, Desplaces A, Manfait M. Characterization of acidic vesicles in multidrug-resistant and sensitive cancer cells by acridine orange staining and confocal microspectrofluorometry. The journal of histochemistry and cytochemistry: official journal of the Histochemistry Society. 1997; 45:1255–1264. [PubMed: 9283613]

Mira L, Fernandez MT, Santos M, Rocha R, Florencio MH, Jennings KR. Interactions of flavonoids with iron and copper ions: a mechanism for their antioxidant activity. Free radical research. 2002; 36:1199–1208. [PubMed: 12592672]

Paglin S, Hollister T, Delohery T, Hackett N, McMahill M, Sphicas E, Domingo D, Yahalom J. A novel response of cancer cells to radiation involves autophagy and formation of acidic vesicles. Cancer research. 2001; 61:439–444. [PubMed: 11212227]

Paranjpe R, Gundala SR, Lakshminarayana N, Sagwal A, Asif G, Pandey A, Aneja R. Piper betel leaf extract: anticancer benefits and bio-guided fractionation to identify active principles for prostate cancer management. Carcinogenesis. 2013; 34:1558–1566. [PubMed: 23430955]

Quideau S, Deffieux D, Douat-Casassus C, Pouysegu L. Plant polyphenols: chemical properties, biological activities, and synthesis. Angewandte Chemie. 2011; 50:586–621. [PubMed: 21226137]

Reagan-Shaw S, Nihal M, Ahmad N. Dose translation from animal to human studies revisited. FASEB journal: official publication of the Federation of American Societies for Experimental Biology. 2008; 22:659–661. [PubMed: 17942826]

Sakihama Y, Cohen MF, Grace SC, Yamasaki H. Plant phenolic antioxidant and prooxidant activities: phenolics-induced oxidative damage mediated by metals in plants. Toxicology. 2002; 177:67–80. [PubMed: 12126796]

Sarkar D, Saha P, Gamre S, Bhattacharjee S, Hariharan C, Ganguly S, Sen R, Mandal G, Chattopadhyay S, Majumdar S, Chatterjee M. Anti-inflammatory effect of allylpyrocatechol in LPS-induced macrophages is mediated by suppression of iNOS and COX-2 via the NF-kappaB pathway. International immunopharmacology. 2008; 8:1264–1271. [PubMed: 18602073]

Sasidharan S, Chen Y, Saravanan D, Sundram KM, Yoga Latha L. Extraction, isolation and characterization of bioactive compounds from plants' extracts. African journal of traditional, complementary, and alternative medicines: AJTCAM/African Networks on Ethnomedicines. 2011; 8:1–10.

Sauer H, Wartenberg M, Hescheler J. Reactive oxygen species as intracellular messengers during cell growth and differentiation. Cellular physiology and biochemistry: international journal of experimental cellular physiology, biochemistry, and pharmacology. 2001; 11:173–186.

Schumacker PT. Reactive oxygen species in cancer cells: live by the sword, die by the sword. Cancer cell. 2006; 10:175–176. [PubMed: 16959608]

Surh YJ. Cancer chemoprevention with dietary phytochemicals. Nature reviews Cancer. 2003; 3:768–780.

Surh YJ. Xenohormesis mechanisms underlying chemopreventive effects of some dietary phytochemicals. Annals of the New York Academy of Sciences. 2011; 1229:1–6. [PubMed: 21793832]

Szatrowski TP, Nathan CF. Production of large amounts of hydrogen peroxide by human tumor cells. Cancer Res. 1991; 51:794–798. [PubMed: 1846317]

Tait SW, Green DR. Mitochondria and cell death: outer membrane permeabilization and beyond. Nature reviews Molecular cell biology. 2010; 11:621–632.

Trachootham D, Alexandre J, Huang P. Targeting cancer cells by ROS-mediated mechanisms: a radical therapeutic approach? Nature reviews. Drug discovery. 2009a; 8:579–591. [PubMed: 19478820]

Trachootham D, Alexandre J, Huang P. Targeting cancer cells by ROS-mediated mechanisms: a radical therapeutic approach? Nat Rev Drug Discov. 2009b; 8:579–591. [PubMed: 19478820]

Highlights

Upon treating human prostate cancer PC-3 cells with hydroxychavicol (HC), our observations suggested that,

- HC perturbs cell-cycle progression by induction of reactive oxygen species (ROS).
- HC mediated cytotoxicity by ROS-induced DNA damage leading to apoptosis.
- HC induced ROS-mediated autophagic response.
- It inhibited prostate tumor growth by ~72% without any observable toxicity.
- Its anticancer efficacy is likely due to its selective prooxidant activity.

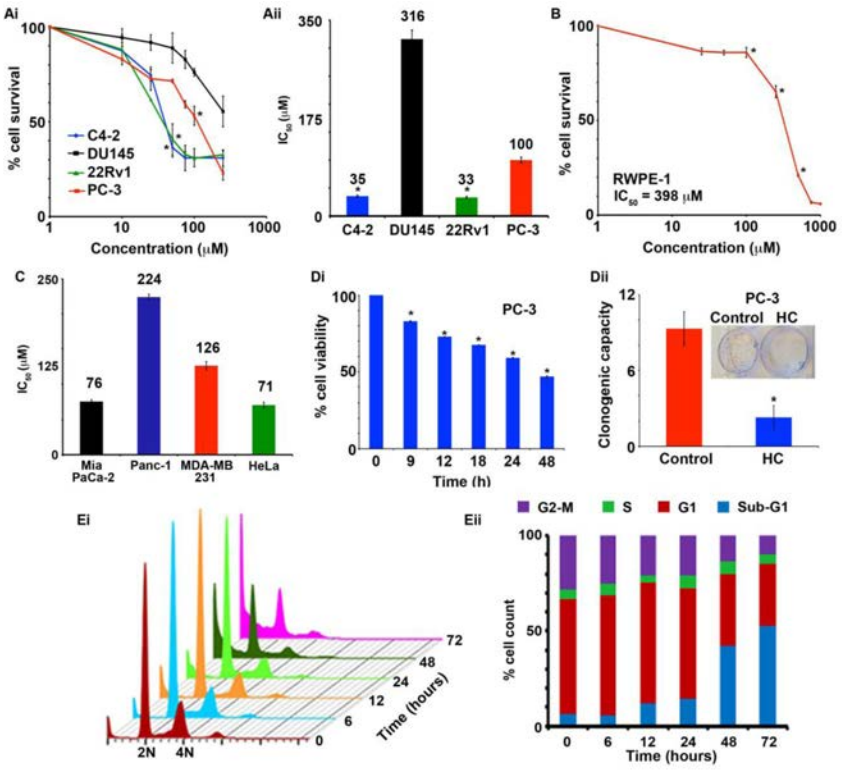

Figure 1. HC inhibits proliferation and perturbs the cell cycle progression of human prostate cancer cells

(Ai) Determination of IC_{50} of HC. PC-3 cells were treated with HC at increasing concentrations (1–250 μM) for 48 h. The percentage cell proliferation was measured by MTT assay. **(Aii) HC shows enhanced inhibition of proliferation in various prostate cancer cells**. Bar-graphical representation of IC_{50} values (mentioned above) of HC tested in C4-2, DU145, 22Rv1, and PC-3 cells. Cells were treated for 48 h with increasing gradient concentrations of HC. The percentage of cell proliferation was measured by MTT assay. **(B) HC does not effect the proliferation of normal cells.** The normal prostate epithelial, RWPE, cells were treated with increasing concentrations of HC and the percent cell proliferation was determined by MTT assay. **(C) HC shows inhibits the proliferation of various cancer cells**. Bar-graphical representation of IC_{50} values (mentioned above) of HC tested in MiaPaCa-2, Panc1, MDA-MB 231, and HeLa cells. Cells were treated for 48 h with increasing gradient concentrations of HC. The percentage of cell proliferation was measured by MTT assay. **(Di) HC effects the cell viability of PC-3 cells.** Bar graphical representation of percent cell viability of PC-3 cells treated with HC as demonstrated by trypan blue assay, (*, $P<0.05$, compared with controls). **(Dii) HC inhibits the clonogenic capacity of prostate cancer cells.** Bar-graphical representation and photograph of crystal violet-stained surviving colonies from control and HC-treated groups. **(E) HC perturbs the cell cycle progression of prostate cancer cells. (Ei)** Cell cycle distribution of PC-3 cells in a three-dimensional disposition as determined by flow cytometry at different time points upon treatment with 100 μM HC. **(Eii)** Bar-graphical representation of the percent G2-M, S, G1 and Sub-G1 populations at different time points. Values and error bars shown in the graphs represent mean and SD respectively. (*, $P<0.05$, compared with controls).

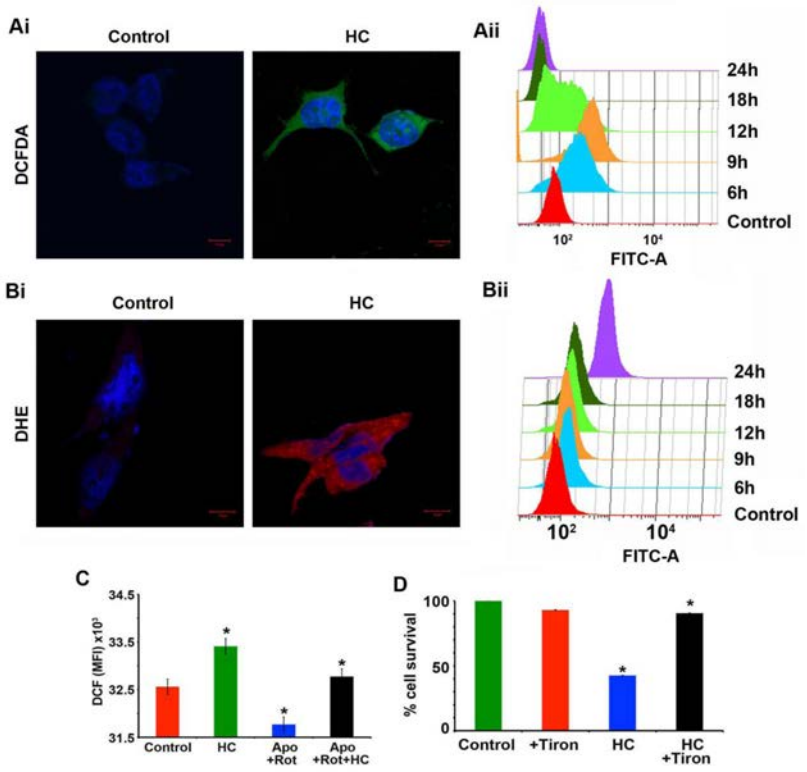

Figure 2. HC induces reactive oxygen species in prostate cancer cells

(Ai) Fluorescent micrographs of DCDA stained-control and HC-treated cells (blue – nucleus; green-DCFDA). **(Aii)** Flow cytometric evaluation of DCFDA stained-control and HC-treated cells at various timepoints. **(Bi)** Fluorescent micrographs of DHE stained-control and HC-treated cells (blue – nucleus; red-DHE). **(Bii)** Flow cytometric evaluation of DHE stained-control and HC-treated cells at various timepoints. **(C) Source of HC-induced ROS.** Mean fluorescent intensity quantitation of ROS produced by ROS in the presence and absence of specific inhibitiors, rotenone (mitochondrial electron transport chain) and apocynin (NOX). **(D) Growth inhibition by HC is ROS-dependent.** Cells were treated for 48 h with 100 μM HC in the presence and absence of ROS scavenger, tiron. The percentage of cell proliferation was measured by MTT assay. Values and error bars shown in the graphs represent mean and SD respectively (*, P<0.05, compared with controls).

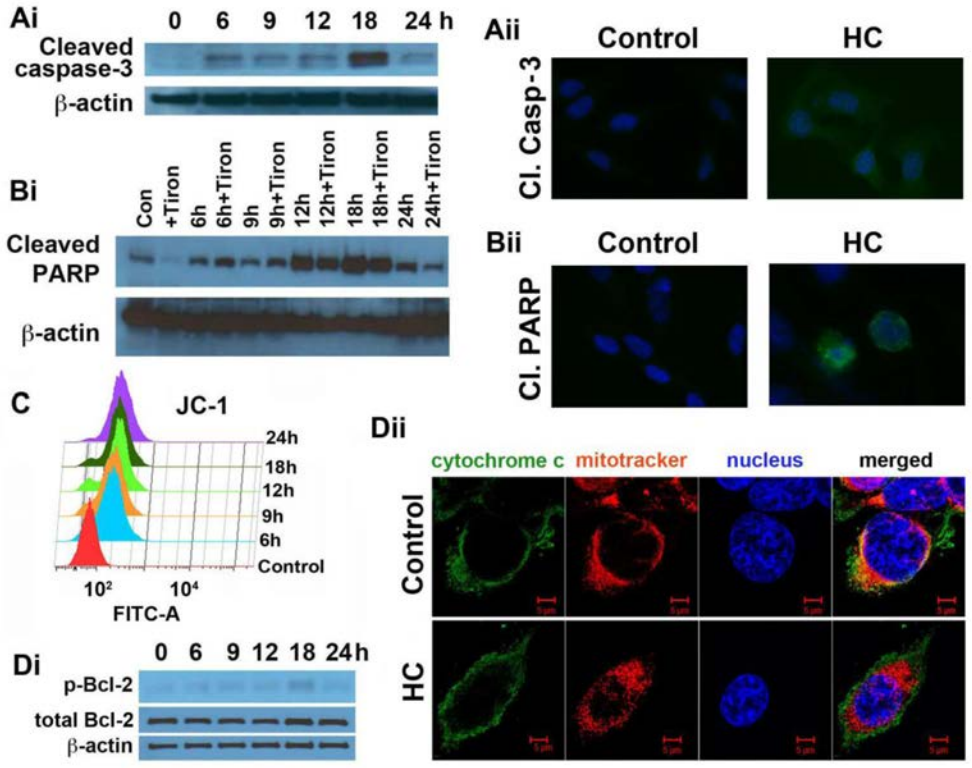

Figure 3. HC induced apoptosis is ROS dependent

Immunoblot and fluorescent microscopic analysis of control and HC-treated cell lysates for apoptotic markers, **(Ai–Aii)** cleaved caspase-3 and **(Bi–Bii)** cleaved PARP, respectively. Cleaved PARP expression was analyzed in the presence and absence of tiron (blue – nucleus; green – cleaved caspase-3 and cleaved PARP). **(C)** HC disrupts the mitochondrial membrane potential in prostate cancer cells. Flow cytometric evaluation of control and HC-treated cells stained with JC-1, a cationic dye. **(Di)** Immunoblot analysis of mitochondrial proteins, p-Bcl-2, and total Bcl-2. β-actin was loading control. (Dii) HC induces release of cytochrome c from mitochondria. Control and HC-treated PC-3 cells were triple stained with MitoTracker (red), which co-localizes in the mitochondria, anti-cytochrome c antibody (green) and Hoechst dye, which stains the nucleus (blue). Overlay of the three stains illustrates the release of cytochrome c from the mitochondria in the HC-treated cells.

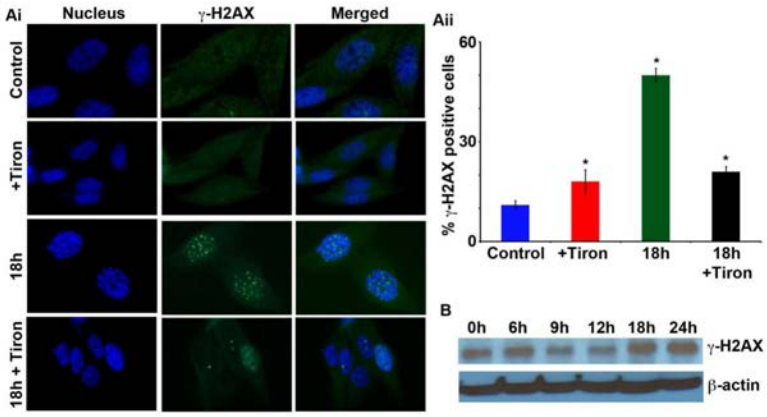

Figure 4. HC induces ROS-dependent DNA damage

(Ai) Immunofluorescent micrographs of control and HC-treated cells stained for γ-H2AX foci in the presence and absence of tiron (blue-nucleus; green-γ-H2AX foci). **(Aii)** Quantitation of the γ-H2AX foci in the micrographs from Ai. **(B)** Immunoblot analysis of γ-H2AX expression in control and HC-treated lysates. β-actin was used as loading control. Values and error bars shown in the graphs represent mean and SD (*, $P<0.05$, compared with controls).

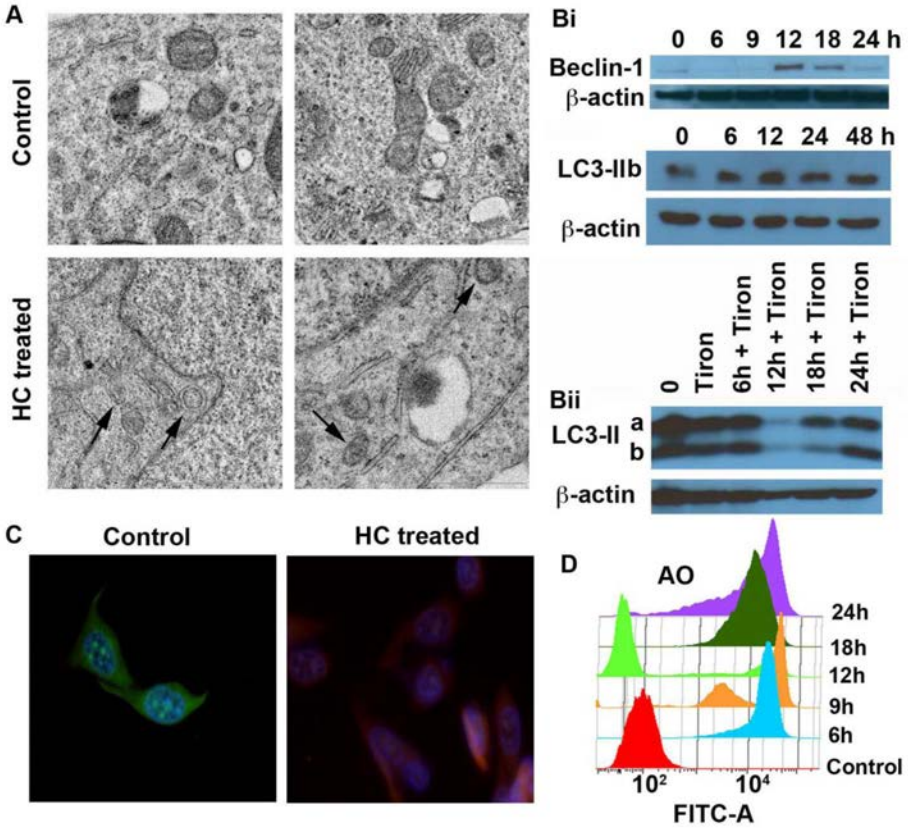

Figure 5. HC induces autophagy in prostate cancer cells

(A) Representative transmission electron micrographs showing the ultrastructures of control and HC-treated PC-3 cells. The double-membranous cytoplasmic vacuoles resembling autophagosomes in HC-treated cells are highlighted by black arrows. Immunoblot analysis of **(Bi)** beclin-1 and LC3-IIb in control and HC-treated cells **(Bii)** LC3-IIb expression in control and HC-treated cells that were pre-treated with tiron. β-actin was loading control. **(C)** Immunofluroscent micrographs of control and HC-treated cells stained with AO (blue – nucleus; green – unprotonated AO; red – AVOs). **(D)** Flow cytometric evaluation of AVOs formation upon treatment with HC at various time points.

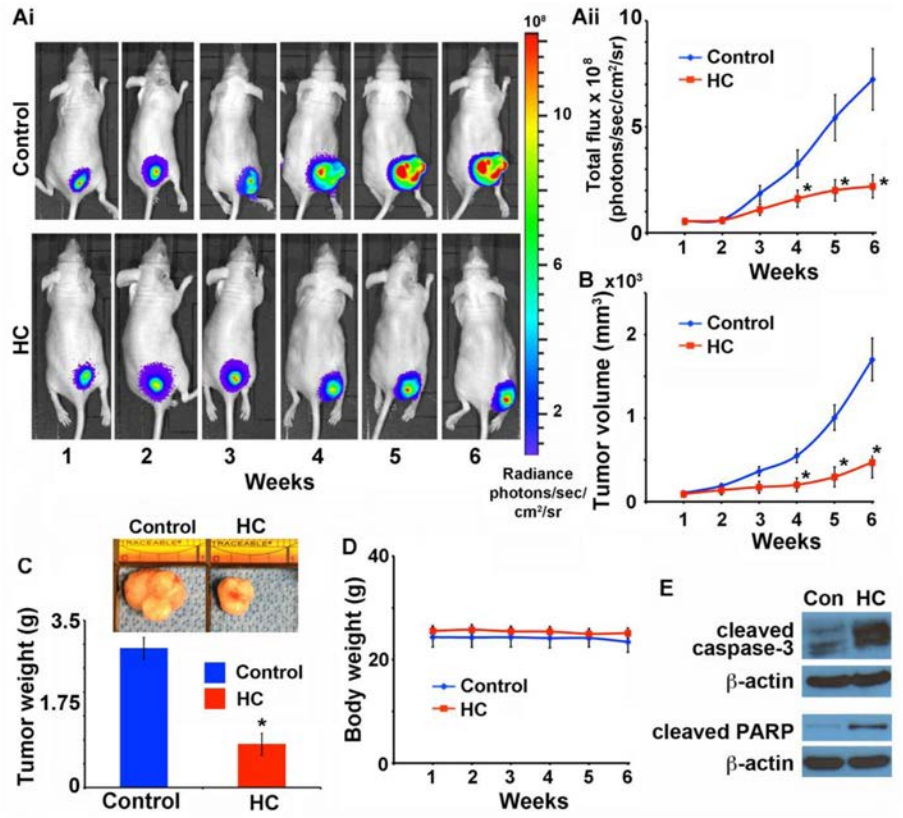

Figure 6. Dietary feeding of HC showed inhibition of human prostate tumor xenograft growth in nude mice

Male nude mice were subcutaneously injected with 10^6 PC-3-luc cells. (**Ai**) Bioluminescent images (one animal per group) representing tumor progression over six weeks. (**Aii**) Quantitation of radiance (photons/sec/cm^2/sr) measured from tumors of vehicle- and HC-fed mice. (**B**) Tumor-volume (in mm^3), (**C**) Tumor weight comparison along with photographic images of excised tumors and (**D**) Body weight comparison of vehicle, and HC-fed groups. (*, P<0.05 (two-way analysis of variance, compared with controls). **(E) HC induces apoptosis.** Immunoblot analysis of tumor tissue lysates from vehicle- and HC-fed groups probed for cleaved caspase-3, and cleaved PARP. β-actin was loading control.